Effects of semiconductor surface band pinning on scanning electrostatic force microscopy

Albert K. Henning [a]

Redwood Microsystems, Inc., 959 Hamilton Avenue, Menlo Park, CA 94025

ABSTRACT

Scanning electrostatic force microscopy, along with a subset of this technique, scanning Kelvin probe microscopy, have been used to explore the materials composition and doping of semiconductor surfaces. Moreover, micromachined semiconductor probes are frequently used in SEFM, SKPM and scanning capacitance microscopy instruments in order to probe the nature of generic surfaces. Some work has been done to explore the electromechanical, and electrostatic nature of the probe-surface interaction for SEFM and SKPM. For instance, it has been demonstrated that band pinning at the semiconductor surface, caused by excessively large values of the *ac* voltage applied between the probe and substrate, creates a false null in an SKPM signal, masking the true nature of the surface.

Recently, results of SEFM probes of semiconductor surfaces have been reported, which used large values of the *ac* voltage applied between the probe and the substrate. In this work, we demonstrate theoretically the effects of both large-signal behavior on the SEFM technique. We also demonstrate the effect of electric field penetration into a semiconductor surface or probe tip on the mechanical response of the probe. The results are compared to measurements, and set in the context of recent work wherein large-signal SEFM techniques are employed.

Keywords: microcantilever; electrostatic force microscopy; EFM; semiconductor cantilever; scanning Kelvin probe microscopy; SKPM; dopant profile; cantilever mechanical transfer function; small signal response; large signal response; surface states; non-linear response.

LIST OF VARIABLES

dU, U_o	*ac* and DC components of applied electrical cantilever excitation (or, electrical bias)
df, f_o	*ac* and DC components of applied mechanical excitation
$F_{elec}(t)$	Electrical force excitation due to applied electrical excitation $U(t)$
$F_{mech}(t)$	Mechanical force excitation
$x(t), v(t)$	Microcantilever displacement, measured as the distance from tip to substrate, and velocity
M, B, K	Effective mass, damping constant, and spring constant for the first normal mode of the microcantilever
Q	Quality factor of the microcantilever resonance
H, W, L	Thickness, width, and length of the microcantilever
H_{tip}, B_{tip}	Height, base diameter of the microcantilever tip
E	Young's modulus for the microcantilever (1.9×10^{11} Pa for silicon)
r	Density for the microcantilever
E_s, y_s	Surface electric field and surface potential (semiconductor band bending)
f_m, f_s	Metal, semiconductor work functions
c_s	Semiconductor electron affinity
A_{eff}	Effective area of electrostatic force interaction between microcantilever and substrate
f_{res}, w_{res}	Resonant frequency of the first normal mode of oscillation of the microcantilever
f_u, w_u	Frequency of the applied electrical excitation
f_f, w_f	Frequency of the applied mechanical excitation
f_u, f_f	Phases of the applied electrical and mechanical excitations
e_s, e_{ins}	Dielectric constant for semiconductor substrate, and for tip-to-substrate dielectric

[a] Email: henning@redwoodmicro.com; WWW: http://www.redwoodmicro.com; Telephone: 650-617-0854; FAX: 650-326-9217

N_f	Surface, fixed charge density of substrate
V_{fb}	Flatband voltage for the microcantilever-substrate system (represents the zero-electrostatic-force condition)
k_B, q, T	Boltzmann's constant, charge of electron, ambient (substrate) temperature
n_0, p_0, n_i	Equilibrium carrier concentrations of electrons and holes, and intrinsic carrier concentration, for the substrate
N_a, N_a^-	p-type dopant concentration, and ionized dopant concentration, in the semiconductor
N_c, N_v	Conduction and valence band densities of states in the semiconductor
E_g, E_a	Semiconductor band gap, and acceptor dopant ionization energy

1.0 INTRODUCTION

Microfabricated cantilevers have become a rich area for research and development. The most obvious application has been in the area of scanned probe microscopy (SPM), which will be the principal focus of this work. However, microfabricated cantilevers have also found application outside of SPM. They have been used as electromechanical "transistors"[1] and as electrostatically-actuated switches.[2] Such devices have been fabricated by using either surface micromachining,[3-5] or bulk micromachining.[6] In these contexts, the distribution of charges on the cantilever as a function of applied bias and mechanical deformation has received important theoretical attention.[7]

In the realm of SPM applications stemming from the use of electrostatic forces between a sensor and a substrate, microfabricated cantilevers have been used as the sensor tip in scanning capacitance microscopy (SCM),[8] scanning electric force microscopy (SEFM),[9] and scanning Kelvin probe microscopy (SKPM).[10] These sensors have been used to detect voltages at microscales on integrated circuits,[11] dopant profiles in semiconductor substrates,[12,13] and charge, material, or structural defects (e.g., grain boundaries) at or near material surfaces.[10,14-16]

Since substrates comprised of semiconductors and related thin film materials are frequently the subject of experimental investigation, it is important to place the theory of force interaction between the cantilever and tip on the firmest theoretical foundation. The electrostatic forces between a charged surface and a semiconductor, without mechanical motion, have been studied.[17,18] The general problems of these force interactions have been addressed in some detail.[10,19]

Typical SPM systems which utilize electrostatic forces involve a cantilever which experiences both a mechanical excitation (in the form of a sinusoidal, piezoelectric driving force) and an electrostatic excitation (in the form of a sinusoidal electrical bias between cantilever and substrate).[20] Also typically, the principal electrostatic force is taken to be exerted by the substrate only on the cantilever tip, though it has been demonstrated experimentally and theoretically that this assumption has limits.[15] When the substrates are semiconductors, the nature of the applied potential between the cantilever and the substrate must receive close attention. For instance, if the *ac* component of the applied potential difference[b] is small, then small-signal analysis applies, and the surface potential in the semiconductor is a well-defined sinusoidal function. In order to increase signal strength, however, some researchers apply external *ac* bias in excess of the semiconductor band gap.[21] Such large *ac* biases require large-signal, non-linear analysis,[22] and in fact disrupt the ability to discern surface potential due to the energy band pinning imposed by such biases.[23] No analysis of the influence of such large-signal, non-linear behavior on the mechanical response of the cantilever has yet been made.

Band pinning caused by large applied *ac* biases is not the only confounding influence on the extraction of quantitative data. From electrostatic SPMs. The presence of significant fixed surface charges can screen electric field coupling between the cantilever and semiconductor, shrouding doping profiles from quantitative analysis.[13,23]

This work extends earlier work[10,13,22,23] by exploring the effect of large applied *ac* biases, between a cantilever and a semiconductor substrate, upon the mechanical response of the cantilever. It adds to this analysis detailed consideration of the impact of surface, fixed charges in the semiconductor.

---

[b] The voltage applied to the cantilever and the substrate contact the respective Fermi levels[24] of these system components. As a result, this applied voltage difference creates an electrochemical potential difference (EPD) between the cantilever and substrate electrical contact points. The EPD is not the same as the surface potential in the semiconductor.[13] This distinction is crucial to understanding electrostatic force couplings in SPM systems having semiconductor components.

2.0 DYNAMIC MICROCANTILEVER MODEL

2.1 Microcantilever structure and mechanical model

Details of the modeling may be found elsewhere.[22] They are summarized here for the sake of completeness. Figure 1 shows a schematic representation of the microcantilever's structural parameters. For simplicity, it is assumed the microcantilever is comprised of silicon, with a thin layer of gold. This structure represents the most general electromechanical case which might be studied. It receives two inputs, $F_{mech}(t)$ and $U(t)$, which vary sinusoidally at different frequencies. The first input is a mechanical force usually imposed by a piezoelectric stack which can excite various normal modes in the distributed mass of the cantilever. The second input is an electrochemical potential difference (EPD), arising from the electrical excitation applied between the cantilever and the substrate.

Figure 2 shows how a lumped element model for the microcantilever's dynamic behavior is extracted from the real system. According to earlier work,[10,19] the first normal mode of oscillation of the microcantilever, the mass, the spring constant, and the damping coefficient, can be found using:

$$\mathbf{v}_{res} = \sqrt{K / M} \qquad K = 4.11 \cdot \frac{WH}{L} \cdot E \qquad M = \boldsymbol{r} \cdot \left(0.24 \cdot WHL + \frac{\boldsymbol{p}}{3} \cdot H_{tip} \cdot \left[\frac{B_{tip}}{2} \right]^2 \right) \qquad B = \frac{M \mathbf{v}_{res}}{Q} \tag{1a-d}$$

The mechanical excitation is then given simply by:

$$F_{mech}(t) = f_0 + df \cdot \sin\left(\mathbf{v}_f t + \boldsymbol{f}_f \right) \tag{2}$$

Typically in SEFM systems, the mechanical excitation is applied at a frequency which is five percent higher than the first or fundamental normal mode of the microcantilever. Similarly, the electrical excitation is:

$$U(t) = U_0 + dU \cdot \sin\left(\mathbf{v}_u t + \boldsymbol{f}_u \right) \tag{3}$$

Finding the electrostatic force from this applied electrical excitation is not straightforward. A primary task of the theory is to quantify the electrostatic force using the structural and materials aspects of the microcantilever-substrate system, as well as the boundary conditions imposed by ambient temperature and the external excitations.

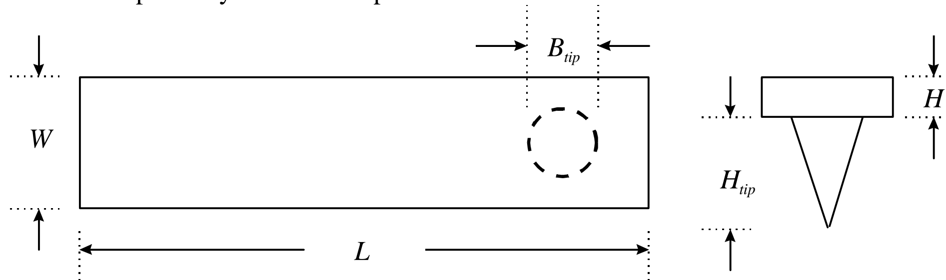

***Figure 1**: Schematic model of a microfabricated cantilever sensor, showing definitions of structural parameters.*

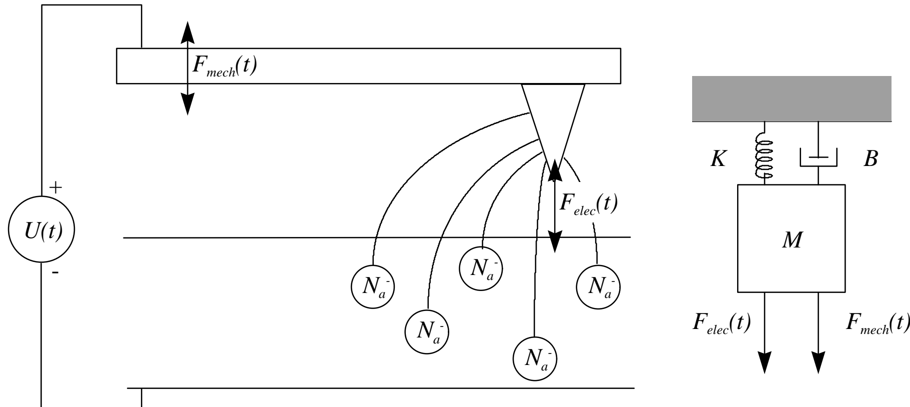

***Figure 2**: Left: Schematic model of a microfabricated cantilever sensor, showing electrostatic forces between the sensor and substrate. Right: Lumped element electromechanical model of the sensor.*

2.2 Energy band diagrams and electrostatic theory.

In order to accomplish this task, we must consider the energy band diagram associated with the microcantilever-substrate system. We confine ourselves to a one-dimensional treatment of the energy bands. The situation is similar to the common metal-insulator-semiconductor (MIS) device which lies at the heart of modern microelectronics.[24] The addition of mechanical motion of the cantilever, however, creates important differences from that device. Again, details may be found elsewhere,[22] and the necessary machinery to move forward is summarized here.

Figure 3 shows the one-dimensional energy band diagram associated with a MIS structure. Note that in a SEFM or SKPM system, the insulator thickness *x(t)* is a function of time, as is required for determination of the microcantilever's dynamic motion. The electrical excitation is applied at the Fermi levels of the microcantilever and substrate, as is also denoted in Figure 2. Using the definitions of the work functions as shown in the figure, a relationship between the applied electrical excitation and the surface potential can be obtained:

$$U(t) = V_{fb} + \boldsymbol{y}_s(t) + \frac{x(t)}{\boldsymbol{e}_{ins}} \cdot \boldsymbol{e}_s E_s\left[\boldsymbol{y}_s(t)\right] \tag{4}$$

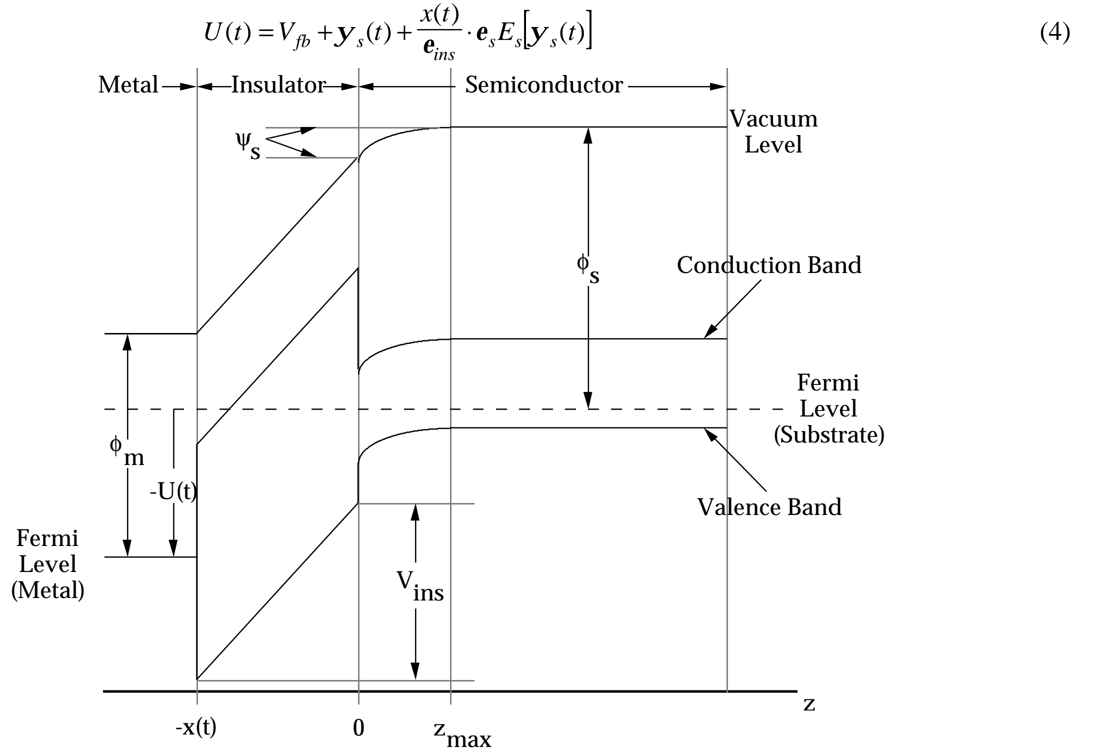

***Figure 3**: One-dimensional energy band diagram used in developing the equations of motion.*

Using Equations (3) and (4) together, the surface potential $\boldsymbol{y}_s(t)$ can be obtained at any time *t*, for a given value of *x(t)*. However, several details remain to be given. The flatband voltage V_{fb} must be determined. If there is surface charge on the semiconductor, then Figure 3, and the application of Gauss' Law at *x*=0 (that is, the continuity of the displacement vector at the insulator-semiconductor interface), yield:

$$V_{fb} = \boldsymbol{f}_m - \boldsymbol{f}_s - qN_f \cdot \frac{x(t)}{\boldsymbol{e}_{ins}} \tag{5}$$

Neglecting the effect of free carriers, the semiconductor work function is given by:[13]

$$\boldsymbol{f}_s = \boldsymbol{c}_s + E_g + \frac{k_B T}{2}\ln\left(N_c / N_v\right) + k_B T \ln\left(\frac{-1 + \sqrt{1 + 16\left(N_a / N_v\right)\exp\left(E_a / k_B T\right)}}{8\exp\left(E_a / k_B T\right)}\right) \tag{6}$$

Note that the flatband voltage represents the conditions of *zero force* between the microcantilever and the semiconductor substrate. This condition is essential to SKPM, where the DC electrical bias U_0 is adjusted until the flatband condition is reached. This condition is *measured* in the SKPM system, which detects the microcantilever deflection at the frequency of

the applied electrical excitation. When the dynamic response of the microcantilever to this excitation is minimized or nulled, the flatband condition has been found. The value of U_0 then contains important information concerning the doping density (through the semiconductor work function $\boldsymbol{f}_s$, which is related logarithmically to the doping density) in the detection volume of the microcantilever tip.[13] However, as seen in Equation (5), and as discussed subsequently in this work, surface charges N_f can obscure extraction of doping concentration using this technique.

The surface electric field can then be related to the surface potential, or band bending, in the semiconductor, using:[24]

$$E_s(\boldsymbol{y}_s) = \mathrm{sgn}(\boldsymbol{y}_s)\cdot E_0 \cdot \sqrt{\exp(-\boldsymbol{by}_s) + \boldsymbol{by}_s - 1 + \frac{n_0}{p_0}\cdot\left[\exp(\boldsymbol{by}_s) - \boldsymbol{by}_s - 1\right]} \qquad \boldsymbol{b} = \frac{q}{k_B T} \qquad E_0 = \sqrt{\frac{qp_0}{\boldsymbol{be}_s}} \tag{7}$$

In this expression, $n_0 p_0 = n_i^2$, and the value of p_0 is set by the ionized dopant concentration outside of the band-bending region. To complete the picture, we need an expression, based on Equation (7), which allows determination of the electrostatic force between the microcantilever and the substrate. Several means are available,[22] but the simplest relies on Figure 2. The total electrostatic force can be thought of as the sum of electric lines of force, emanating from the microcantilever tip, over an effective area of interaction A_{eff}, which terminate on *bulk* charges, and on *surface* charges. The electrostatic force due to bulk charges can be shown to be:

$$F_{bulk}(E_s) = A_{eff}\,\boldsymbol{e}_s E_s^{\,2} \tag{8}$$

The electrostatic force due to surface charges can then be shown to be:

$$F_{surface}(E_s) = \frac{A_{eff}}{2\boldsymbol{e}_{ins}}\left\{\boldsymbol{e}_s^2 E_s^2 - 2q\boldsymbol{e}_s N_f E_s + q^2 N_f^2\right\} \tag{9}$$

Note that the portion of the electrostatic force due to bulk charges is always attractive, while the portion due to surface charges can be either attractive or repulsive, depending upon the charge nature of the fixed surface charges, or of the Fermi-level-dependent surface states, which give rise to the force.

3.0 DYNAMIC RESPONSE

3.1 Equations of microcantilever motion when sensing a semiconductor substrate.

We now have completed laying out the machinery necessary to perform analysis of effects of doping, surface charge, and the magnitude of the applied electrical excitation. The analysis is founded on the state variable equations of mechanical motion for the microcantilever-substrate system, which are:

$$\frac{dv}{dt} = \frac{1}{M}\left\{F_{mech}(t) - Bv - Kx - F_{elec}(t)\right\} \tag{10}$$

$$\frac{dx}{dt} = v \tag{11}$$

Note the sign of $F_{elec}(t)$; it acts to attract the microcantilever to the substrate, while positive values of $F_{mech}(t)$ act to pull the two apart. $F_{mech}(t)$ is given simply by Equation (2). $F_{elec}(t)$ must be found in a more circuitous fashion. First, at a given value of $x(t)$, Equations (3), (4) and (5) must be solved self-consistently for $\boldsymbol{y}_s(t)$. Then, the surface electric field $E_s(\boldsymbol{y}_s)$ is found using Equation (7). Finally, Equations (8) and (9) are combined to deliver the electrostatic force:

$$F_{elec}(t) = F_{bulk}(E_s) + F_{surface}(E_s) \tag{12}$$

These equations must in most cases be solved numerically, since two important non-linearities are present. First, the electrostatic force has an inverse dependence on $x(t)$, as seen in Equation (4): $F_{elec}(t)$ is proportional to E_s^2 and E_s, and the surface field is inversely proportional to the displacement between the microcantilever and the substrate. Second, for a semiconductor substrate the surface potential becomes 'pinned' by the semiconductor conduction or valence band, if the applied electrical excitation is too large. As a consequence, the electrostatic force also reaches a maximum or saturation value, regardless of the *ac* or DC magnitudes of $U(t)$.

3.2 Equations of microcantilever motion when sensing a metal substrate.

Equations (10) and (11) have been presented with a semiconductor substrate in mind. They are, however, completely general, with respect to the nature of the substrate material. It can be either a metal, a semiconductor, or an insulator containing fixed surface charge. If the substrate is a metal, then the surface potential and surface electric field in the

substrate are zero, and all lines of electric force between the microcantilever tip and the substrate terminate on surface charges (which are, in this case, mobile, but still represented by N_f). So:

$$F_{elec,metal} = F_{surface} = \frac{A_{eff}}{2\mathbf{e}_{ins}}\left\{q^2 N_f^2\right\} \tag{13}$$

But, *U(t)* is related to the surface charge using Equations (4) and (5). So, the electrostatic force becomes:

$$F_{elec,metal}(t) = \frac{A_{eff}\,\mathbf{e}_{ins}}{2x^2}\cdot\left[\mathbf{f}_m - \mathbf{f}_s - U(t)\right]^2 \tag{14}$$

4.0 RESULTS AND DISCUSSION

4.1 Questions under consideration, and previous results.

This work seeks to answer several questions relating to the use of SEFM or SKPM in monitoring semiconductor surfaces for information about dopant density,[13] or about the values of potentials applied in the substrate[21]. First, does the application of large electrical biases, which result in band pinning of the surface potential, obscure the extraction of quantitative information about the potential distribution, or the charge distribution, in the substrate detection volume, *neglecting* effects of such biases on the microcantilever sensor motion? Second, does the application of large electrical excitations, in excess of the band gap of the semiconductor, affect the dynamic response of the microcantilever? That is, do large electrical signals create non-linear motion in the microcantilever sensor? Third, does the presence of surface charge, from fixed or surface state sources, affect the dynamic microcantilever response, and/or screen the extraction of quantitative data about the substrate?

Some experimental observations and theoretical analyses have been made relating to these questions. Experimentally, in Ref. 23 it was shown that increasing the *ac* component of the applied electrical excitation *U(t)* in an SKPM system resulted in loss of information about the nature of the work function difference between the microcantilever tip and substrate. This result is presented here in Figure 4 for reference.

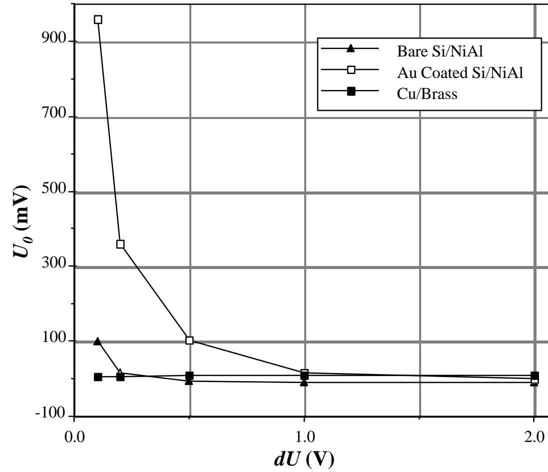

***Figure 4**: Measured dependence of V_{fb} on the magnitude of dU.*

This result is understood in the context of Figure 5. Here, the surface potential at room temperature in a semiconductor substrate with a *p*-type doping concentration of 10^{16} cm^{-3} is shown, in response to applied electrical excitations *U(t)* of varying strength. The calculations are for an SEFM system with a gold-coated microcantilever, held mechanically rigid at a fixed cantilever-to-substrate distance of 10 nm. The value of U_0 is set equal to V_{fb}, so that, in the absence of *dU*, the microcantilever will experience no force. Due to the band pinning of the surface potential in the semiconductor, the waveforms associated with small and large values of *dU* are, respectively, linear and non-linear. The non-linear waveform has a mean, or average, value which is non-zero over the period of the applied sinusoidal electrical excitation, which leads to the expectation that U_0 will have to be adjusted *away from* its true value, in order to null or minimize the electrostatic force sensed by the microcantilever. It remains to be seen whether this expectation holds when the microcantilever is allowed to move.

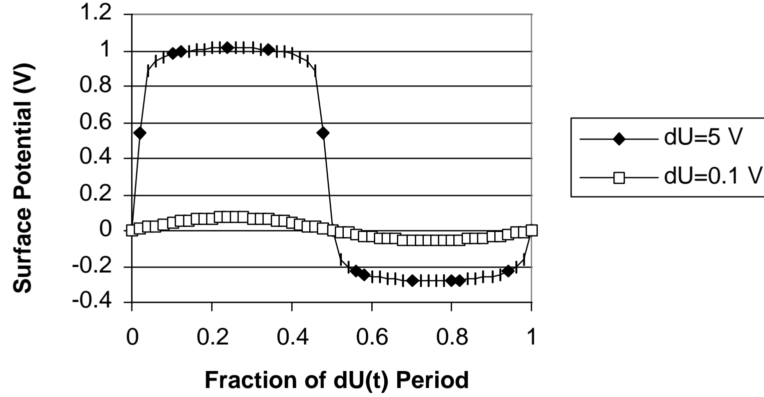

***Figure 5**: Simulation of time-dependent response of semiconductor surface potential, as a function of dU.*

4.2 Effects of non-linearities due to band pinning.

We extend the results of Section 4.1, to cover the full range of dopant densities and applied bias ranges which may be experienced in an SEFM or SKPM system. Figure 6 shows the value of ψ_s, averaged over one cycle of the applied bias $U(t)$. For this simulation, U_0 is set to V_{fb}, and N_f=0. So, if dU is zero, then flatband is achieved, no electrostatic force exists between the microcantilever and the substrate, and the average value of ψ_s averaged over one cycle will be zero. If dU is small enough, then the system is still linear and symmetric, and the value of ψ_s averaged over one cycle will remain zero. Departures from linearity will result, however, if there is band pinning, and the electrostatic force becomes non-symmetric. Such non-linearities can be seen in Figures 6-8. The $\log_{10}$ doping concentrations are shown in the legends. Figure 6 shows the departure from a zero mean value of surface potential as dU is increased, while Figure 7 shows the same result for the electrostatic force. Figure 8 shows the shift in microcantilever average position, as determined by dividing the average value of the electrostatic force over one cycle by the spring constant K. If the value of this *ac* displacement dx were nulled or minimized, as occurs in a true SKPM system, then U_0 would have to shift from the true flatband condition.

These figures show several other important details. First, under flatband conditions, application of *ac* bias in excess of 0.5 V causes significant departure of the surface potential from a mean value of zero. Application of such biases in excess of 1 V causes similar departures for electrostatic force, and for mean microcantilever displacement (the laser-measured component in the SEFM or SKPM system). Second, not surprisingly the system is more sensitive to higher doping concentrations. Accordingly, lower values of dU can be used at higher doping concentrations, in order to preserve the linearity of the system. This result contrasts with SCM, where sensitivity is highest for low doping concentrations, and lowest at high doping concentrations.[8] Finally, recall our assumption that the doping concentration is uniform in the substrate. In terms of the SEFM and SKPM measurements techniques, in truth these methods *average* the doping concentration in the detection volume. This volume is defined by the lateral extent of the electrostatic field, and the depletion depth z_{max} in the vertical direction (see Figure 3). Small values of dU minimize this depletion depth, and ensure extracted doping profiles are true surface profiles, unobscured by subsurface effects.

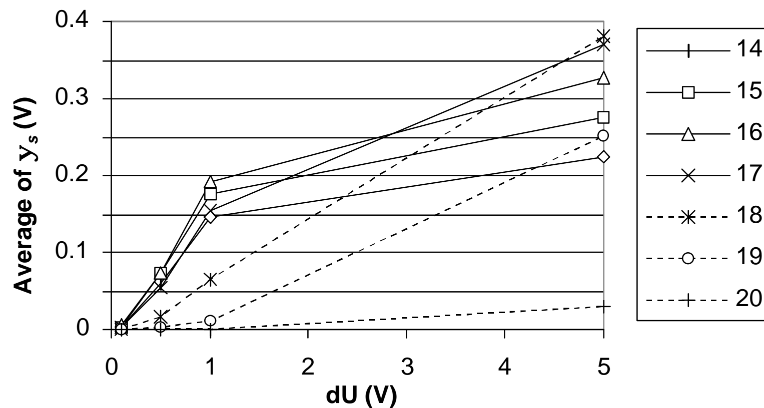

***Figure 6**: Shift in mean semiconductor surface potential over one cycle of U(t), as a function of dU.*

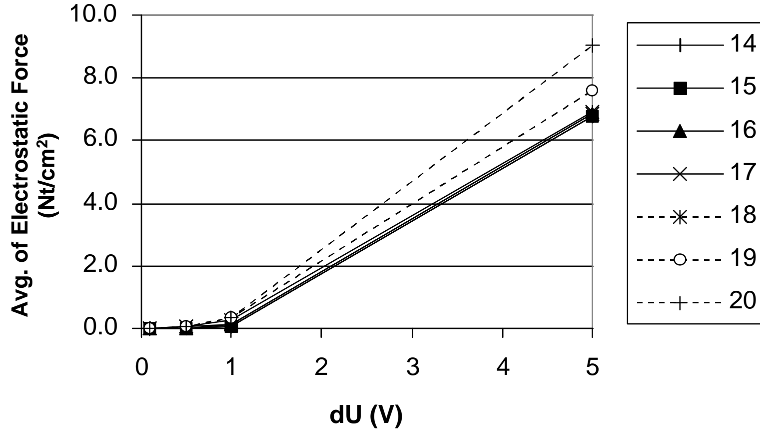

***Figure 7**: Shift in mean microcantilever force over one cycle of U(t), as a function of dU.*

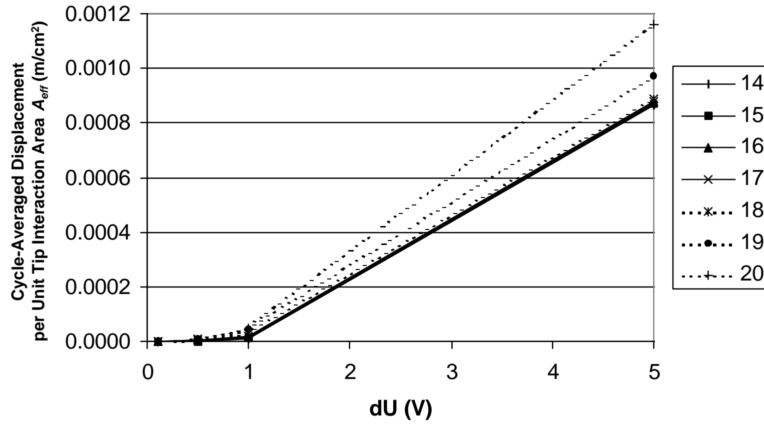

***Figure 8**: Shift in mean microcantilever position over one cycle of U(t), as a function of dU. [Note: The shifts are negative in value, but are plotted here as positive-definite for clarity.]*

4.3 Effects of non-linearities due to response of the microcantilever to mechanical and electrical excitations.

We seek next to reconcile these results, with an analysis that includes the dynamic mechanical response of the microcantilever to the applied external excitations. A number of assumptions are used in applying the one-dimensional theory to a three-dimensional system. The only electrostatic forces between the microcantilever tip and the substrate are assumed to be through an effective area A_{eff} associated with the microcantilever tip.[15] The microcantilever is assumed to be comprised of silicon, coated with a thin layer of gold, so that its electrical interaction with the substrate is governed by the gold, but its dynamic mechanical properties are determined by the crystalline silicon. The semiconductor substrate is assumed to be *p*-type silicon, with a uniform dopant concentration in the substrate volume of interaction between the tip and substrate, so that Equation (6) can hold. Atomic forces between the microcantilever and the substrate are ignored.

The constants used in the next simulations are as follows: N_a=10^{16} cm^{-3}; $\boldsymbol{r}$=2339 kg/m^3; W=20 μm; H=5 μm; L is adjusted so that f_{res}≈600 kHz; H_{tip}=7 μm; B_{tip}=3 μm; Q=10; $\boldsymbol{w}_f$=1.05$\boldsymbol{w}_{res}$; both applied excitation phases $\boldsymbol{f}_u$ and $\boldsymbol{f}_f$ are set to zero; f_u=100 kHz.

Figure 9 shows the mechanical response of the microcantilever represented by these constants, in the absence of any electrical excitation. The frequency of the applied mechanical excitation is seen to be about 560 kHz. f_0 and df are adjusted so that the equilibrium displacement of the cantilever is about 10 nm, and the magnitude of the displacement oscillation is set to about 0.5 nm, in the absence of electrostatic forces. These values are consistent with observations from a physical SKPM system.[10]

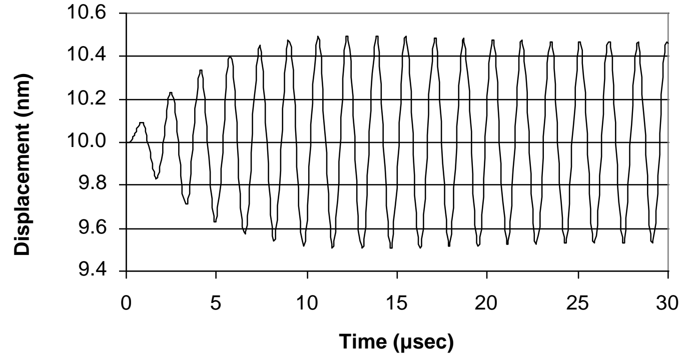

***Figure 9**: Mechanical response of the microcantilever in the absence of electrical excitation.*

Figures 10-13 show mechanical microcantilever displacement, and electrostatic force, as a function of time for a variety of electrical excitation conditions. In Figure 10, the DC component of the electrical bias is equal to the flatband condition. The *ac* component is small. These conditions should produce a linear response in the displacement. However, as seen in the displacement plot, the microcantilever displacement is dominated by the mechanical excitation. The magnitude of the electrostatic force, and the effective area of interaction between the tip and the substrate, are insufficient to produce much detectable mechanical oscillation at the frequency of the electrical excitation.

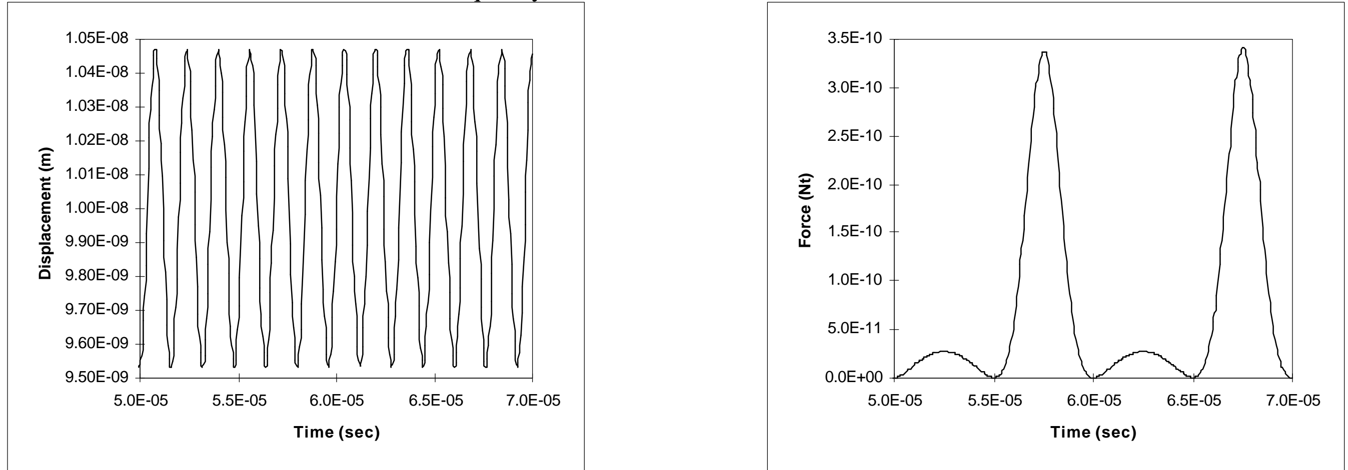

***Figure 10**: Displacement and force for the following conditions:* $A_{eff}=3.3\ \mu m^2$; $U_0=V_{fb}$; $dU=0.1$ V; $N_a=10^{16}\ cm^{-3}$; $N_f=0$.

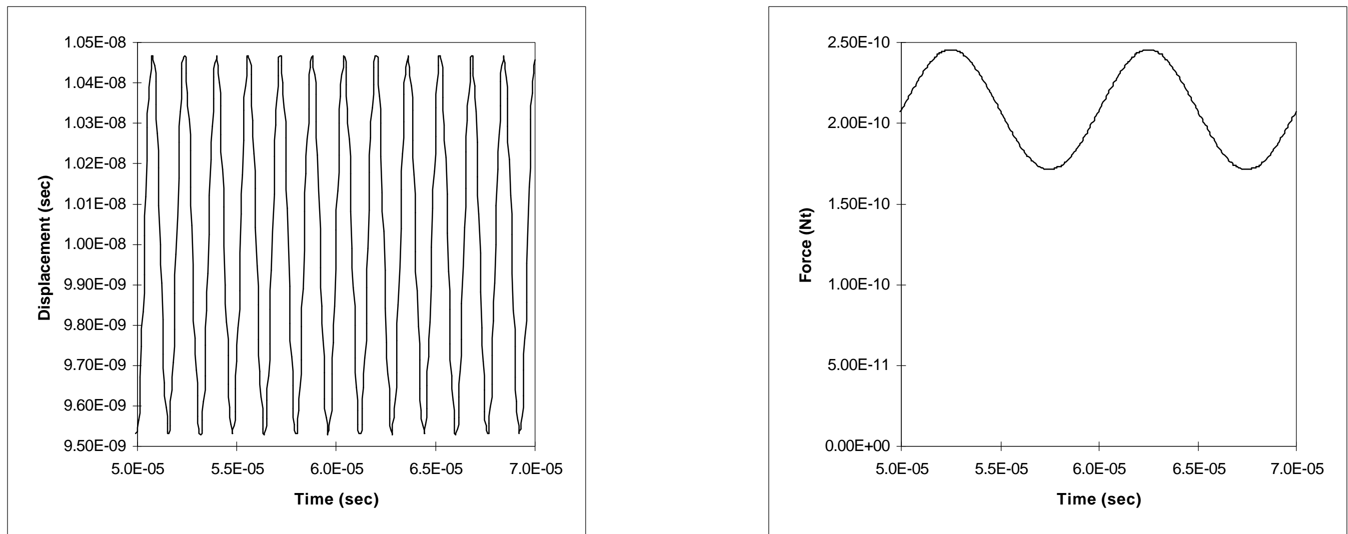

***Figure 11**: Displacement and force for the following conditions:* $A_{eff}=3.3\ \mu m^2$; $U_0=0.5$ V; $dU=0.1$ V; $N_a=10^{16}\ cm^{-3}$; $N_f=0$.

Figure 11 repeats the conditions of Figure, but with U_0 no longer at the flatband condition. The electrostatic force is seen to vary sinusoidally (at *twice* the frequency of the applied electrical excitation, since F_{elec} is proportional to E_s^2). However, its average value is higher than in Figure 10, reflective of the nonlinearity imposed by high values of $U(t)$. Again, as in Figure 10, the electrostatic coupling is insufficient in strength to deliver measurable (to the eye) displacement at the frequency of the electrical excitation.

We can increase this displacement by increasing the magnitude of the electrostatic force, but only at the expense of non-linearities in the displacement of the microcantilever sensor. Figure 12 repeats the conditions of Figure 10, with U_0 again at the flatband condition, but dU increased to 1.0 V. Now a distinct displacement is observed, at the electrical excitation frequency. However, the displacement is highly nonlinear, and has higher-frequency components which occur due to both the nonlinear nature of the surface potential, and the $1/x$ nature of the electrostatic force coupling to the microcantilever. Especially, the attractive electrostatic force *increases* as x decreases – a positive-feedback effect which results in so-called 'tip crashes' in actual SKPM or SEFM systems, where the electrostatic force pulls the tip down until physical contact with the substrate is made.

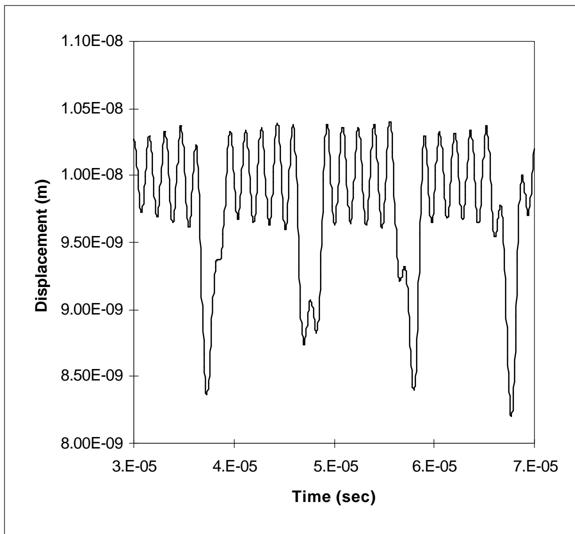

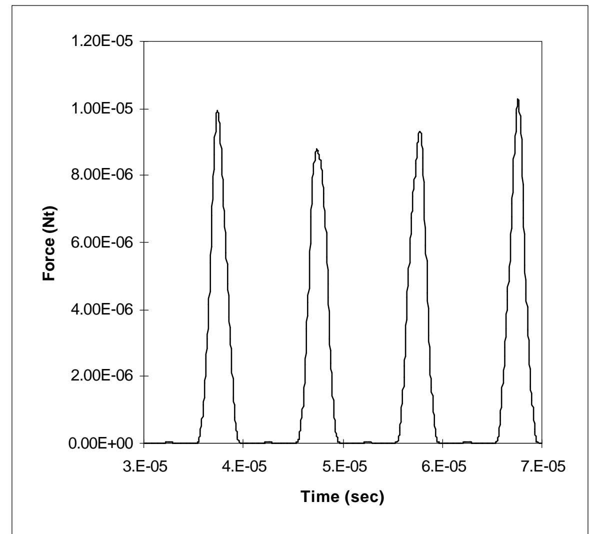

***Figure 12**: Displacement and force for the following conditions:* A_{eff}=3.3 μm^2; $U_0=V_{fb}$; dU=1.0 V; $N_a=10^{16}$ cm^{-3}; N_f=0.

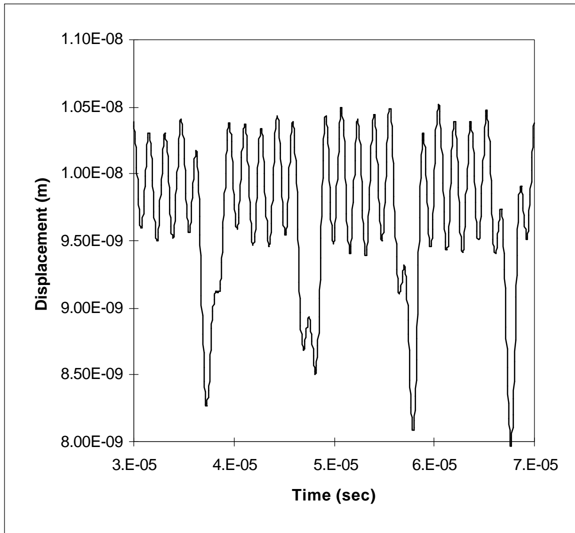

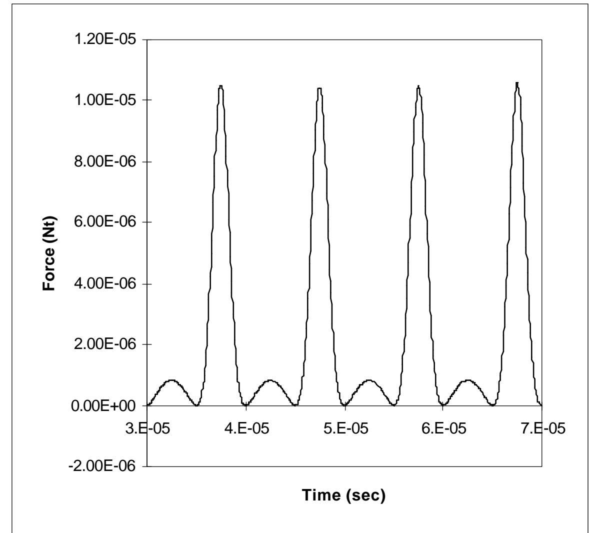

***Figure 13**: Displacement and force for the following conditions:* A_{eff}=(316 μm)^2; $U_0=V_{fb}$; dU=0.1 V; $N_a=10^{16}$ cm^{-3}; N_f=0.

4.4 Effects of surface charge.

The effect of surface charge, due to either fixed charges or surface states, in a microcantilever-semiconductor substrate system, are seen most clearly in Equation 5. N_f causes shifts in flatband voltage, which depend upon the dielectric constant between the microcantilever tip and the substrate, as well as on the distance between the tip and substrate. Unfortunately, increasing the microcantilever detection sensitivity by decreasing the mean position of the tip relative to the substrate, causes increases in screening due to the surface charge. For the system explored in greatest depth in this work, where the insulator is air, and mean displacement is 10 nm, Table 1 shows the apparent shift in the flatband voltage which results from surface charges of different densities. Also shown is the effect of moving the microcantilever probe closer to the surface. In this instance, such a change diminishes the effect of N_f on V_{fb}. Surface charge densities of up to 10^{11}-10^{12} cm^{-2} can be tolerated, with minimal impact on V_{fb}.

$\log_{10}(Nf)$	x_0 (nm)	ΔV_{fb} (V)	x_0 (nm)	ΔV_{fb} (V)
9	10	1.81E-05	5	9.03E-06
10	10	0.000181	5	9.03E-05
11	10	0.001806	5	0.000903
12	10	0.018059	5	0.009029
13	10	0.180587	5	0.090293
14	10	1.805869	5	0.902935

***Table 1**: Effect of surface charge on apparent shift in V_{fb}.*

5.0 CONCLUSIONS

The effects of electrostatic and mechanical forces on micro-fabricated cantilevers have been presented. The effects of work function differences between the cantilever and substrate, and fixed charge on semiconductor substrate surfaces, have been incorporated. The analysis makes no small-signal assumptions for either mechanical motion or applied bias, and therefore is most general. The analysis has been limited to a study of a lumped element model for the fundamental mode of oscillation of a vibrating cantilever, though higher order modes may be incorporated. Dynamic responses for mechanically fixed and mechanically free systems have been presented, for metal-semiconductor electrostatic coupling. The results show that values of *ac* electrical excitation in excess of 0.5 to 1.0 V will obscure the ability of an SKPM or SEFM system to discern surface potential, or to extract quantitative information about the doping concentration. Higher doping concentrations provide greater electrostatic force coupling, allowing use of lower *ac* electrical detection biases. Placing the microcantilever sensor closer to the substrate increases sensitivity at low values of dU, but at the expense of increased susceptibility to non-linearities in the dynamic motion of the microcantilever. Microcantilever motion displays non-linearities which depend upon the strength of the applied electrical bias, the magnitude of the applied mechanical excitation, the doping concentration, and the equilibrium displacement between the cantilever sensor and the substrate.

6.0 ACKNOWLEDGEMENTS

The author acknowledges gratefully collaborations with Charles P. Daghlian, Todd Hochwitz, Christopher G. Levey, and James A. Slinkman on earlier portions of this work.

7.0 REFERENCES

1. H. C. Nathanson and R. A. Wickstrom, “A resonant-gate silicon surface transistor with high-Q bandpass properties.” *Appl. Phys. Lett.* **7**, pp. 84-86 (1965).
2. P. M. Zavracky, N. E. McGruer, and S. Majumder, “Micromechanical switches.” *J. Microelectromech. Syst.* **6**, pp. 3-9 (1997).
3. T.A. Core, W.K. Tsang, and S.J. Sherman, “Fabrication technology for an integrated surface-micromachined sensor.” *Sol. St. Tech.* **36**, pp. 39-40 (1993).
4. W.C. Tang, T.-C.H. Nguyen, M.W. Judy, and R.T. Howe, “Electrostatic-comb drive of lateral polysilicon resonators.” *Sens. and Act.* **A21**, pp. 328-331 (1990).
5. M.W. Judy, Y.-H. Cho, R.T. Howe and A.P. Pisano, “Self-adjusting microstructures (SAMS).” In *Proceedings, IEEE Micro Electro Mech. Syst.* (IEEE, New York, 1991), pp. 51-56.

6. K. Petersen, “Silicon as a mechanical material.” *Proc. IEEE* **70**(5), pp. 420-457 (1982).
7. P. Osterberg, H. Yie, X. Cai, J. White, and S. Senturia, “Self-consistent simulation and modelling of electrostatically deformed diaphragms.” In *Proceedings, IEEE Micro Electro Mech. Syst. Conf.* (IEEE, Piscataway, NJ, 1994), pp. 28-32; P.M. Osterberg, *Electrostatically Actuated Microelectromechanical Test Structures for Material Property Measurement*. Ph.D. dissertation (Massachusetts Institute of Technology, Cambridge, MA, 1995).
8. C. C. Williams, W. P. Hough, and S. A. Rishton, “Scanning capacitance microscopy on a 25 nm scale.” *Appl. Phys. Lett.* **55**, pp. 203-205 (1989).
9. Y. Martin, D. W. Abraham, H. K. Wickramasinghe, “High-resolution capacitance measurement and potentiometry by force microscopy.” *Appl. Phys. Lett.* **52**, pp. 1103-1105 (1988).
10. T. Hochwitz, *Implementation, Characterization, and Applications of a Scanning Kelvin Probe Force Microscope.* Ph.D. dissertation (Dartmouth College, Hanover, NH, 1996).
11. R. A. Said, G. E. Bridges, and D. J. Thomson, “Scanned electrostatic force microscope for noninvasive high frequency potential measurement.” *Appl. Phys. Lett.* **64**, pp. 1442-1444 (1994); J. N. Nxumalo, D. Shimizu, and D. J. Thomson, “Cross-sectional imaging of semiconductor device structures by scanning resistance microscopy.” In *Proceedings, 3rd Intl. Workshop on the Measurement and Characterization of Ultra-Shallow Doping Profiles in Semiconductors* (American Vacuum Society, New York, 1995)
12. C. C. Williams, J. Slinkman, W. P. Hough, and H. K. Wickramasinghe, “Lateral dopant profiling with 200 nm resolution by scanning capacitance microscopy.” *Appl. Phys. Lett.* **55**, pp. 1662-1664 (1989).
13. A. K. Henning, T. Hochwitz, J. Slinkman, J. Never, S. Hoffman, P. Kaszuba, and C. P. Daghlian, “Two-dimensional surface dopant profiling in silicon using scanning Kelvin probe microscopy.” *J. Appl. Phys.* **77**, pp. 1888-1896 (1995).
14. T. Hochwitz, A. K. Henning, C. P. Daghlian, R. Gluck , R. Bolam, P. Coutu, and J. Slinkman, “DRAM failure analysis with the force-based Kelvin probe.” In *Proceedings, Int’l. Reliability Physics Symposium*, pp. 217-222 (IEEE, Piscataway, NJ, 1995).
15. T. Hochwitz, A. K. Henning, C. G. Levey, C. P. Daghlian, J. Slinkman, “Capacitive effects on quantitative dopant profiling with scanned electrostatic force microscopes.” In *Proceedings, Third Intl. Workshop on the Measurement and Characterization of Ultra-Shallow Doping Profiles in Semiconductors*, pp. 51.1-51.9 (American Vacuum Society, New York, 1995); T. Hochwitz, A. K. Henning, C. G. Levey, C. P. Daghlian, J. Slinkman, “Capacitive effects on quantitative dopant profiling with scanned electrostatic force microscopes.” *Journal of Vacuum Science and Technology* **B14**, pp. 457-462 (1996).
16. T. Hochwitz, A. K. Henning, C. G. Levey, C. P. Daghlian, J. Slinkman, James Never, Phil Kaszuba, Randy Wells, John Pekarik, Bob Gluck, “Imaging dopant profiles of integrated circuit devices with the force-based scanning Kelvin probe microscope.” In *Proceedings, Third International Workshop on the Measurement and Characterization of Ultra-Shallow Doping Profiles in Semiconductors*, pp. 47.1-47.8 (American Vacuum Society, New York, 1995); T. Hochwitz, A. K. Henning, C. G. Levey, C. P. Daghlian, J. Slinkman, James Never, Phil Kaszuba, Randy Wells, John Pekarik, Bob Gluck, “Imaging dopant profiles of integrated circuit devices with the force-based scanning Kelvin probe microscope.” *Journal of Vacuum Science and Technology* **B14**, pp. 440-446 (1996).
17. C. Donolato, “Electrostatic problem of a point charge in the presence of a semi-infinite semiconductor.” *J. Appl. Phys.* **78**, pp. 684-690 (1995).
18. S. Hudlet, M. Saint Jean, B. Roulet, J. Berger, and C. Guthmann, “Electrostatic forces between metallic tip and semiconductor surfaces.” *J. Appl. Phys.* **77**, pp. 3308-3314 (1995).
19. D. Sarid, *Scanning Force Microscopy with Applications to Electric, Magnetic, and Atomic Forces.* (Oxford University Press, New York, 1991).
20. M. Nonnenmacher, J. Greschner, O. Wolter, and R. Kassing, “Scanning force microscopy with micromachined silicon sensors.” *J. Vac. Sci. Tech.* **B9**, pp. 1358-1362 (1991).
21. T. Mizutani, M. Arakawa, and S. Kishimoto, “Two-dimensional potential profile measurement of GaAs HEMT’s by Kelvin probe force microscopy.” *Elec. Dev. Lett.* **18**, pp. 423-425 (1997).
22. A. K. Henning, “Effects of doping on the dynamic mechanical reponse of semiconductor cantilevers to electrostatic forces.” In *Proceedings, Microlithography and Metrology in Micromachining* (International Society for Optical Engineering, Bellingham, WA, 1995; M. T. Postek, ed.), volume 2640, pp. 236-245.
23. A. K. Henning and T. Hochwitz, “Scanning probe microscopy for 2-D semiconductor dopant profiling and device failure analysis.” *Materials Science and Engineering* **B42**, pp. 88-98 (1996).
24. S. M. Sze, *Physics of Semiconductor Devices*. (2nd edition, John Wiley & Sons, New York, 1981).